Desalination and Water Treatment
www.deswater.com

doi: 10.5004/dwt.2022.28851

272 (2022) 118–125
October

Competitive adsorption of alkali metal ions onto Prussian blue

Tan Guo[a,*], Shan Yun[a], Yuan Liang[a], Jiahui Li[a], Yanxing Li[a], Xiushen Ye[b,*], Zhijian Wu[b]

[a]*National and Local Joint Engineering Research Center for Deep Utilization Technology of Rock-Salt Resource, Faculty of Chemical Engineering, Huaiyin Institute of Technology, No. 1 Meicheng Road, Huai'an 223003, China, Tel. +86 517 83559720; emails: guotan@hyit.edu.cn (T. Guo), yunshan@hyit.edu.cn (S. Yun), l1933469740@163.com (Y. Liang), ljh19816090257@163.com (J. Li), liyanxing@hyit.edu.cn (Y. Li)*
[b]*Qinghai Institute of Salt Lakes, Chinese Academy of Sciences, No. 18 Xinning Road, Xining 810008, China, Tel. +86 971 6307871; emails: yexs@isl.ac.cn (X. Ye), zjwu@isl.ac.cn (Z. Wu)*

Received 13 April 2022; Accepted 17 August 2022

ABSTRACT

Prussian blue (PB) is an effective adsorbent for separating Cs^+. However, the competitive adsorption behavior of alkali metal ions onto PB was unknown, and the Cs^+ adsorption mechanism of the PB was controversial. In this work, the adsorption behaviors of alkali metal ions onto prepared PB were investigated in single-element and multi-element solutions. The equilibrium adsorption capacity was in the sequence of $Cs^+ > Rb^+ > Na^+$, while Li^+ and K^+ were not adsorbed. Kinetic curves of Na^+, Rb^+ and Cs^+ were all better fitted with the pseudo-second-order kinetics model. The adsorption isotherms data of Rb^+ and Cs^+ agreed with the Freundlich model while Na^+ followed the Langmuir model. It was found that the mechanism for the adsorption of M^+ (Na^+, Rb^+ and Cs^+) onto PB was H^+-exchange and K^+-exchange according to $\Delta C\ (M^+) = \Delta C\ (K^+) + \Delta C\ (H^+)$.

Keywords: Cesium; Competitive adsorption; Ion exchange; Prussian blue; Rubidium

1. Introduction

Rubidium (Rb) and cesium (Cs) are expensive and extremely important metal resources, which play an important role in many fields such as medical treatment, photoelectric devices, metal ion catalysts, communication, aviation and ceramic industry, etc. In nature, in addition to the minerals lepidolite and pollucite, Rb and Cs are reserved considerably in salt lake brine, geothermal water and oilfield water [1]. However, these liquid resources of Rb and Cs are still far from being fully explored. The chemical composition of salt lake brine is complex and the main components are Na^+, K^+, Li^+, Mg^{2+}, Cl^- and SO_4^{2-} with a high concentration. On the other hand, the physical and chemical properties of Rb^+ and Cs^+ are very similar to that of Na^+, K^+ and Li^+, particularly the hydrated cation radius [2], which makes it difficult to separate rubidium and cesium with low concentration. Therefore, it is very important to develop an efficient method for separation and extraction of Rb and Cs in salt lakes.

Currently, the separation of Rb and Cs mainly includes precipitation method [3], solvent extraction [4] and adsorption [5,6]. The precipitation method is not suitable for separating Rb^+ and Cs^+ with low concentrations in salt lake brine due to poor efficiency, low purity of the product and high cost [7,8]. Although solvent extraction can be used to remove Rb^+ and Cs^+ quickly [9,10], the extractant and diluent will corrode the equipment and pollute the environment during the extraction process. Adsorption has the advantages of a high recovery rate, excellent separation effect, pollution-free and low energy consumption suitable for the separation of low concentration target ions in salt lake brine compared with precipitation and solvent extraction. In particular, low-cost and stable Prussian

* Corresponding authors.

blue (PB), a kind of ferrocyanide, has been effectively used as one of the most promising adsorbents to separate Cs^+ [11,12]. At present, many researches mainly focus on the elimination of Rb and Cs from radioactive waste liquid [13–15], and there are few studies on the competitive adsorption of alkali metal ions aimed at salt lake brine. Moreover, the mechanism of Cs^+ adsorption onto PB is still a controversial subject. Up to now, there are two different viewpoints reported about adsorption mechanisms, the one is Cs^+ adsorbed onto PB by exchange with H^+, Na^+, K^+ [16,17], and the other is Cs^+ incorporated into PB crystalline structure as an ion-pair with anion [18,19].

In order to understand the alkali metal ions adsorption mechanism in the competitive system, the adsorbent of PB was synthesized, and the competitive adsorption properties, the kinetic curves and isothermal performances were conducted via batch adsorption experiments in this work.

2. Experimental section

2.1. Materials

Lithium chloride (LiCl), sodium chloride (NaCl), potassium chloride (KCl) and potassium hexacyanoferrate ($K_4[Fe(CN)_6]$) were purchased from Tianjin Baishi Chemical Industry Co., Ltd., China. Rubidium chloride (RbCl), cesium chloride (CsCl) and iron(III) chloride ($FeCl_3$) were supplied by Sinopharm Chemical Reagent Co., Ltd., China. All reagents were analytical grade without further purification. All aqueous solutions were prepared with distilled water.

2.2. Synthesis of Prussian blue

PB was synthesized by addition of 50 mL 0.6 mol L^{-1} aqueous solution of $K_4[Fe(CN)_6]$ to 40 mL 1 mol L^{-1} aqueous solution of $FeCl_3$ under vigorously stirring for 10 min. The resulting blue slurry was separated via filtration by a vacuum pump and washed several times with distilled water. Finally, the separated precipitate was allowed to dry in a drying oven to obtain the powder of PB adsorbent and then carefully ground using an agate mortar.

2.3. Characterization of materials

The elemental composition of the PB samples was observed by an Oxford INCA energy dispersive spectroscopy (EDS, Oxford Instruments Ltd., UK). X-ray diffraction (XRD, PANalytical, Netherlands) measurements were conducted with an X'Pert PRO diffractometer using Cu-K_α radiation at 40 kV and 30 mA over a 2θ range from 5° to 70°. X-ray photoelectron spectrometry (XPS, Thermo Fisher Scientific Ltd., USA) was performed with an ESCALAB 250Xi. The SEM analysis was got using Hitachi Regulus8100, and the PB sample was coated with Au using Oxford Ultim Max 65. Surface area of PB powder was performed using a Micromeritics ASAP 2460.

2.4. Adsorption experiments

0.1 g PB was added into 10 mL alkali metal ion solution (ranging from 4 to 100 mmol L^{-1} for each metal ion) in a sealable plastic tube, stirred using a SHA-C shaker (Changzhou Guohua Co., Ltd., China) under constant conditions (25°C, 155 rpm). The concentration of the alkali metal ions was investigated using an Optima7000DV inductively coupled plasma atomic emission spectrometry (ICP-AES, PerkinElmer Ltd., USA). The adsorption capacity (q, mmol g^{-1}) of the alkali metal ions onto PB was calculated by Eq. (1), where C_0 (mmol L^{-1}) and C (mmol L^{-1}) are the concentration of alkali metal ions at the beginning t_0 and time t, respectively, V (L) is the volume of the solution, and m (g) is the mass of the PB adsorbent.

$$q = \frac{V\left(C_0 - C\right)}{m} \tag{1}$$

To understand the rate of adsorption, the equilibrium adsorption capacity, the detailed adsorption behavior and adsorption mechanism, the adsorption kinetics and isotherm models were studied. Linear pseudo-first-order and pseudo-second-order kinetic models corresponding to Eqs. (2) and (3), respectively, were used to investigate the kinetic behavior of alkali metal ions on PB, where t (h) is the contact time, k_1 (h^{-1}) and k_2 (g $mmol^{-1}$ h^{-1}) are the adsorption rate constants, and q_t and q_e (mmol g^{-1}) are the adsorption capacity at time t and equilibrium, respectively.

$$\ln\left(q_e - q_t\right) = \ln q_e - k_1 t \tag{2}$$

$$\frac{t}{q_t} = \frac{1}{k_2 q_e^2} + \frac{t}{q_e} \tag{3}$$

Langmuir and Freundlich isotherms were described using linear forms of Eqs. (4) and (5), respectively, where C_e (mmol L^{-1}) is the equilibrium concentration of alkali metal ions in the solution, q_m (mmol g^{-1}) is the maximum adsorption capacity of PB, b (L $mmol^{-1}$) is the Langmuir isotherm parameter, k and n are the Freundlich isotherm parameters.

$$\frac{1}{q_e} = \frac{1}{q_m} + \left(\frac{1}{bq_m}\right)\left(\frac{1}{C_e}\right) \tag{4}$$

$$\lg q_e = \lg k + \frac{1}{n}\lg C_e \tag{5}$$

0.5 g PB adsorbent was mixed with 50 mL salt lake brine in Laguocuo playa of Tibet in China, carried out at 25°C in a water bath with a shaking speed of 155 rpm. The initial (C_0) and equilibrium (C_e) concentration of the metal ions in salt lake brine were determined using an ICP-AES.

3. Results and discussion

3.1. Characterization of PB

Fig. 1a shows the XRD pattern of PB, whose characteristic diffraction peaks at 17.5°, 24.6°, 35.2° and 40.0° corresponded to the (200), (220), (400) and (420) crystal planes,

respectively [13,20]. Oxygen and potassium existed in the PB crystal from EDS pattern as shown in Fig. 1b, revealing there being crystallization water molecules and lattice defect sites related to the presence of K^+ from $K_4[Fe(CN)_6]$ [21]. As shown in Fig. 1c, the particle size distribution of PB powder was about several microns to several tens of microns. The BET specifc surface area of PB powder was 160.5305 $m^2 \cdot g^{-1}$ calculated by the Brunauer–Emmett–Teller (BET) method from the N_2 adsorption isotherm data.

3.2. Adsorption kinetics

The adsorption kinetics experiments were carried out to investigate the equilibrium time for the adsorption of Li^+, Na^+, K^+, Rb^+ and Cs^+. As shown in Fig. 2, initially, adsorption capacity increased rapidly with the increase of adsorption time and finally reached a plateau. The adsorption capacity increased in the order of $Li^+ \sim K^+ < Na^+ < Rb^+ < Cs^+$, and Li^+ and K^+ were hardly adsorbed onto PB in the single-element system and multi-element system. Furthermore, PB scarcely adsorbed Na^+ in the multi-element system (Fig. 2b). It was also clear that the adsorption of Na^+, Rb^+ and Cs^+ reached equilibrium at 4, 48 and 48 h, respectively. According to the equilibrium time, the adsorption rate of Rb^+ and Cs^+ was slower than that of Na^+. However, PB showed the highest selectivity toward Cs^+.

From Fig. 2b, the capacity of adsorption as negative values for K^+ gradually decreased with the passage of time. This signified that the elevated concentration of K^+ caused by the release of K(I) (existed in the PB crystal lattice spaces) into the adsorption solution systems.

The experimental kinetics data of Na^+, Rb^+ and Cs^+ were fitted using pseudo-first-order and pseudo-second-order rate models as shown in Fig. 3. The kinetic constants of q_e,

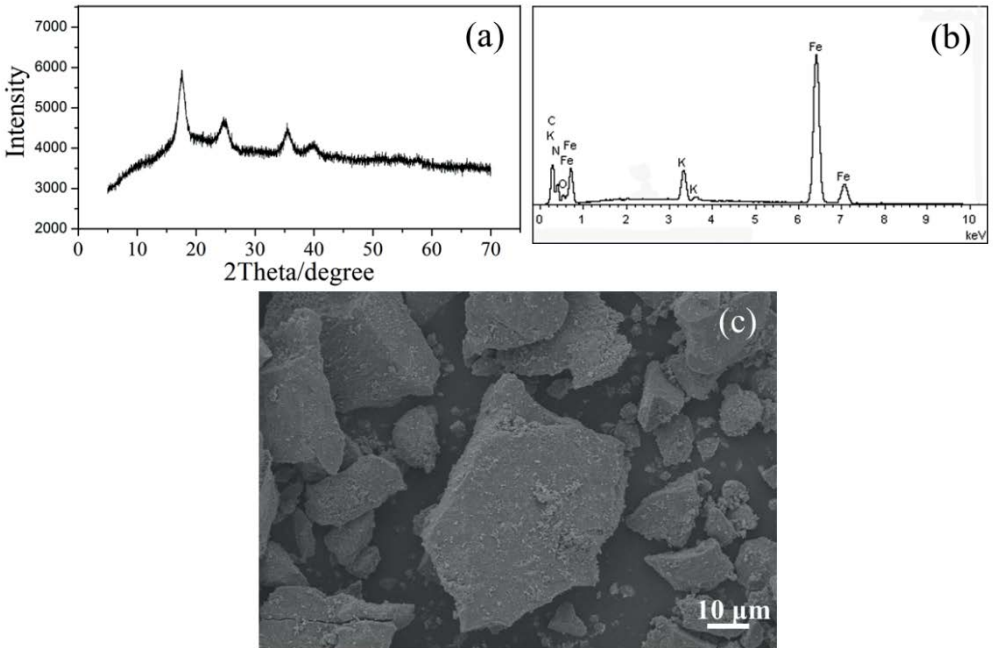

Fig. 1. The XRD pattern (a), EDS pattern (b) and SEM pattern (c) of PB.

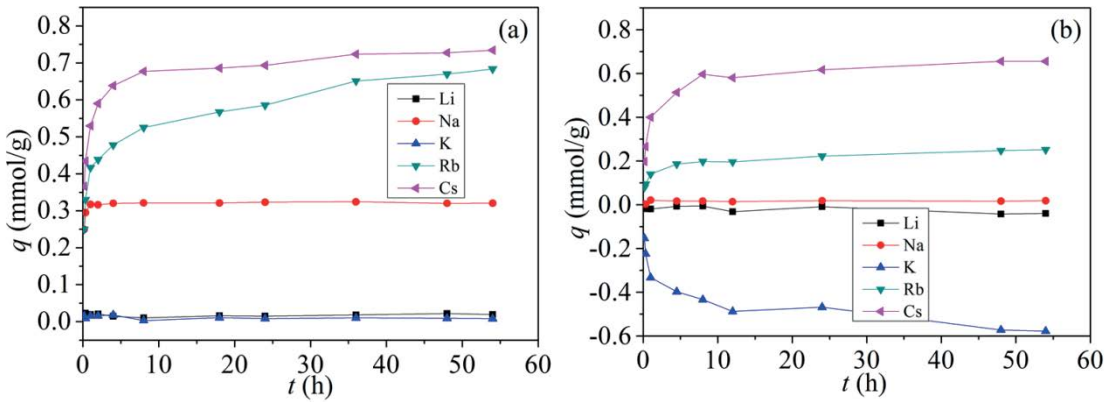

Fig. 2. Effect of time on the adsorption capacity at 25°C in the single-element system (a) and multi-element system (b). Initial concentration of Li^+, Na^+, K^+, Rb^+, Cs^+ = 10 mmol L^{-1}.

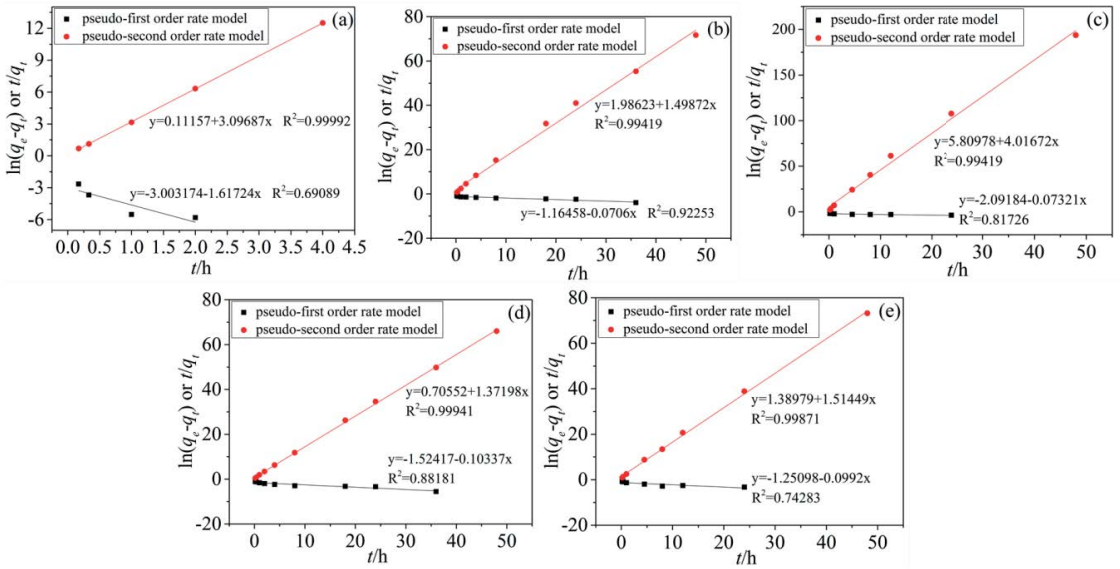

Fig. 3. Fitting curves of pseudo-first-order and pseudo-second-order rate models for Na^+ in single-element solution (a), Rb^+ in single-element solution (b), Rb^+ in multi-element solution (c), Cs^+ in single-element solution (d), and Cs^+ in multi-element solution (e).

Table 1
Kinetic parameters of Na^+, Rb^+ and Cs^+ onto PB at 25°C

System	Metal ion	$q_{e,exp}$ (mmol g^{-1})	Pseudo-first-order model			Pseudo-second-order model		
			$q_{e,cal}$ (mmol g^{-1})	k_1 (h^{-1})	R^2	$q_{e,cal}$ (mmol g^{-1})	k_2 (g $mmol^{-1}$ h^{-1})	R^2
Single-element	Na^+	0.320	0.050	1.62	0.6909	0.323	85.96	0.9999
	Rb^+	0.670	0.312	0.07	0.9225	0.667	1.13	0.9942
	Cs^+	0.727	0.218	0.10	0.8818	0.729	2.67	0.9994
Multi-element	Rb^+	0.248	0.123	0.07	0.8173	0.249	2.78	0.9942
	Cs^+	0.656	0.286	0.10	0.7428	0.660	1.65	0.9987

k_1 and k_2 were calculated based on the intercept and slope of the fitting curves as indicated in Table 1. The correlation coefficients (R^2) for pseudo-first-order kinetics model were lower, which demonstrated that the diffusion was not the rate-determining step [22]. The adsorption processes of Na^+, Rb^+ and Cs^+ all conformed to the pseudo-second-order kinetics model on the basis of the correlation coefficients (Table 1). In addition, the calculated values ($q_{e,cal}$) through the pseudo-second-order model were more consistent with the experimental equilibrium adsorption capacity ($q_{e,exp}$). These results implied that chemisorption was the rate-limiting step [22,23]. Moreover, k_2 of Rb^+ was close to that of Cs^+, and both were slightly small, signifying that the adsorption rate of Rb^+ and Cs^+ onto PB was slower. k_2 of Na^+ was much higher than that of Rb^+ and Cs^+, which agreed with the adsorption equilibrium time of the three ions from Fig. 2.

3.3. Adsorption isotherms

To further understand the adsorption capacity of Na^+, Rb^+ and Cs^+ onto PB, the isotherms experiments with various concentrations of a single metal ion were carried out at 25°C. The equilibrium adsorption capacity was arranged in the following sequence of $Cs^+ > Rb^+ > Na^+$ from the equilibrium adsorption isotherms as illustrated in Fig. 4.

The isotherms were fitted by Langmuir and Freundlich models as depicted in Fig. 5, and the calculated Langmuir and Freundlich constants are shown in Table 2. According to the correlation coefficients, the experimental data of single-element systems for Na^+ was an acceptable fit with the linear plot of the Langmuir model belonged to single layer adsorption, while Rb^+ and Cs^+ were in good agreement with the predicted Freundlich model belonged to multilayer adsorption. The fitting data of q_m (1.36 mmol g^{-1}) correlated well with the experimental results (1.30 mmol g^{-1}). Ordinarily, the higher the n parameters representing the greater adsorption strength, it was generally difficult to adsorb when $n < 0.5$ [22,24]. From Table 2, the value of n being approximately 7 was far larger than 0.5, which meant a favorable adsorption process for Rb^+ and Cs^+ onto PB.

3.4. Adsorption mechanism

3.4.1. Ion exchange mechanism

Fig. 6 shows the XPS spectra of PB before and after adsorption. It can be seen that there were C1s, N1s, O1s,

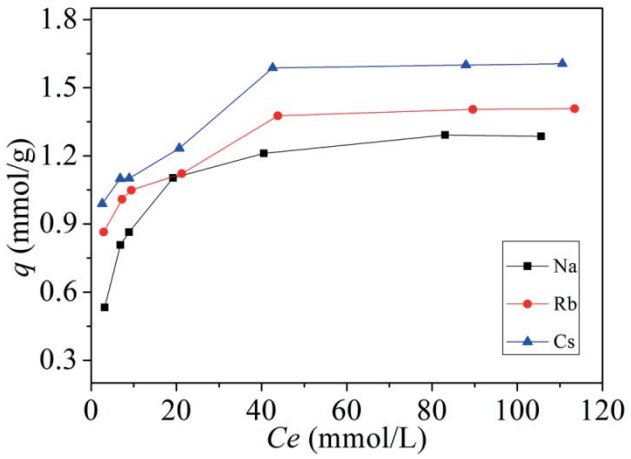

Fig. 4. Adsorption isotherms for single Na^+, Rb^+ and Cs^+ onto PB at 25°C. Initial concentration of Na^+, Rb^+, Cs^+ = 4, 8, 10, 20, 40, 80, 100 mmol L^{-1}.

Fe2p and K2p peaks in the spectra, indicating that K^+ was introduced into PB adsorbent during the preparation process consistent with the EDS characterization. Na1s, Rb3d and Cs3d peaks appear in Fig. 6b–d, respectively, demonstrating Na^+, Rb^+ and Cs^+ effectively adsorbed onto PB. From Fig. 6e, the peak of Cs3d was strong while the peak

Table 2
Isotherm model parameters of single Na^+, Rb^+ and Cs^+ adsorption onto PB at 25°C

Metal ion	Langmuir			Freundlich		
	q_m (mmol g^{-1})	b (L $mmol^{-1}$)	R^2	k	n	R^2
Na^+	1.36	0.203	0.9988	0.486	4.33	0.8601
Rb^+	1.34	0.558	0.8367	0.760	7.25	0.9545
Cs^+	1.47	0.665	0.6625	0.837	6.91	0.9280

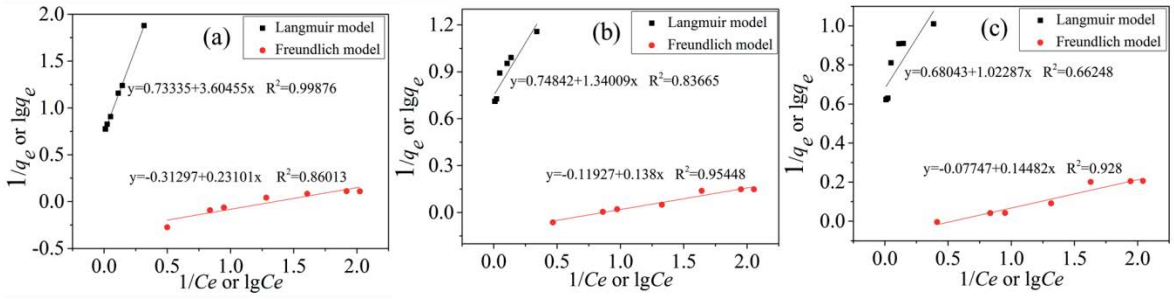

Fig. 5. Adsorption isotherm models for single Na^+ (a), Rb^+ (b) and Cs^+ (c) onto PB.

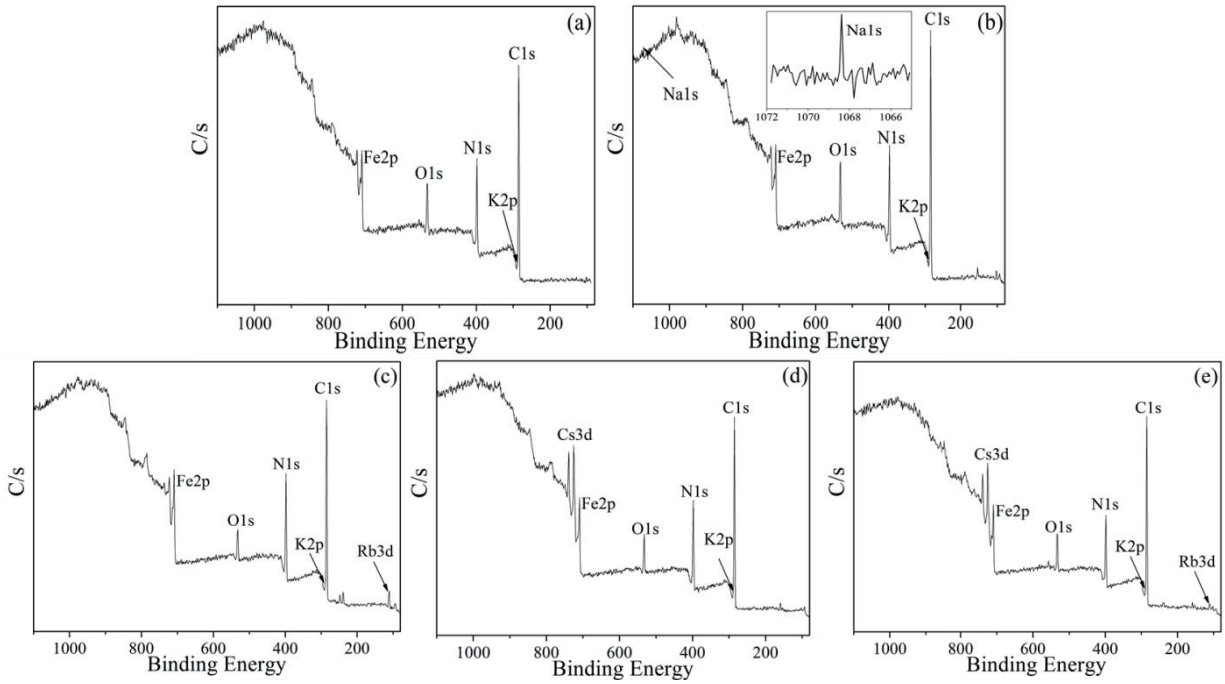

Fig. 6. XPS spectra of PB before adsorption (a), after adsorption single Na^+ (b), after adsorption single Rb^+ (c), after adsorption single Cs^+ (d) and after adsorption multi Na^+, Rb^+ and Cs^+ (e).

of Rb3d was weak, and the peaks of Na and Li were not observed, which was in good agreement with the experimental results of kinetic curves.

Fe^{3+} in the solution of $FeCl_3$ could hydrolyze to produce plenty of H^+. In the process of preparation of PB, H^+ was incorporated in PB lattice to compensate for the negative charges [25,26]. The pH values of the solutions determined by a pH meter (PB-10, Sartorius Scientific Instruments (Beijing) Co. Ltd.) all decreased after adsorption from Table 3, which was due to the ion exchange between H^+ in PB lattice and alkali metal ions in adsorption solution, defining it as a type of H^+-exchange reaction. The concentration of K^+ increased in solution after adsorption, indicating that an ion exchange reaction of K^+ in PB lattice with M^+ (Na^+, Rb^+ and Cs^+) as a type of K^+-exchange. The sum of the increments of H^+ and K^+ was approximately equal to the decrement of alkali metal ions as listed in Table 4. Consequently, the adsorption mechanism of Na^+, Rb^+ and Cs^+ for PB was H^+-exchange and K^+-exchange.

In Fig. 7, it could be seen that the diffraction peak positions were not changed after the alkali ions adsorption. However, the intensity ratios of the (200) crystal plane signal tended to become weaker and wider after the single Cs^+ (Fig. 7d) and multi alkali ions adsorption (Fig. 7e). The XRD diffraction peak intensity of PB with adsorbed Na^+ and Rb^+ was unchanged from Fig. 7b and c. It was likely that Cs^+ could be adsorbed throughout the crystal lattice spaces, while Na^+ and Rb^+ probably sited on the crystal surface without getting into the crystal lattice structure [17].

Little change in the concentration of Cl^- was measured by an ion chromatograph (ICS-1100, Dionex Corporation) from Table 5. Thus, the mechanism of Na^+, Rb^+ and Cs^+ sorption by PB was not attributed to the incorporation of ion pairs with alkali ions and a coordinating anion Cl^- into vacant sites of the PB lattice.

3.4.2. Sieve effect in the ion exchange

As provided in Table 4, ΔC (K^+) was 3.05, 5.00 and 3.20 mmol L^{-1} for Na^+, Rb^+ and Cs^+ in the single-element system, respectively, making clear that the exchange amount between K^+ and Rb^+ was the largest, which may be because of their very similar physicochemical properties [27]. There was almost no ion exchange between H^+ and Na^+, while the ion exchange between H^+ and Cs^+ was more easier according to ΔC (H^+), since the smaller hydration cation radius of Cs^+ may be more suitable for PB lattice spaces in size. The

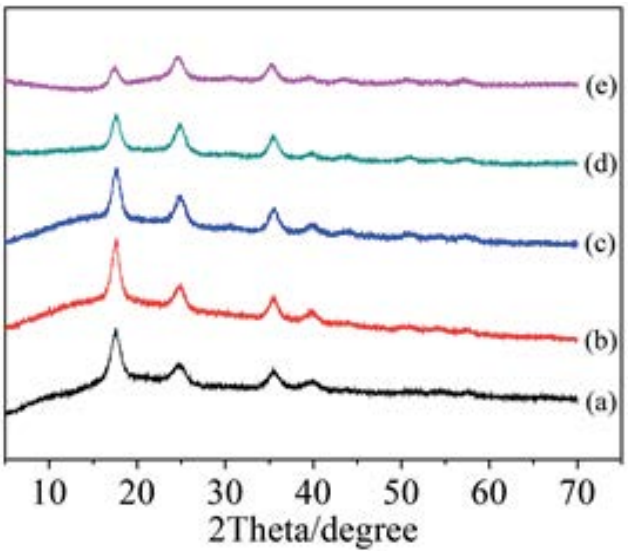

Fig. 7. XRD patterns of PB: Before adsorption (a), after adsorption single Na^+ (b), after adsorption single Rb^+ (c), after adsorption single Cs^+ (d) and after adsorption multi Na^+, Rb^+ and Cs^+ (e).

Table 3
The pH values of adsorption solution

	Single-element system			Multi-element system
	NaCl solution	RbCl solution	CsCl solution	
Before adsorption	6.29	6.58	7.00	6.58
After adsorption	3.48	2.72	2.39	2.47

Table 5
The concentration of Cl^- in adsorption solution before and after adsorption

	Single-element system (mmol L^{-1})			Multi-element system (mmol L^{-1})
	NaCl	RbCl	CsCl	
Before adsorption	11.11	10.52	10.65	48.18
After adsorption	11.76	10.59	10.13	48.62

Table 4
Changes in ion concentration (ΔC) in adsorption solution before and after adsorption

	Single-element system (mmol L^{-1})			Multi-element system (mmol L^{-1})
	NaCl solution	RbCl solution	CsCl solution	
ΔC (M^+)	3.21	6.83	7.34	9.26
ΔC (K^+)	3.05	5.00	3.20	5.78
ΔC (H^+)	0.33	1.89	4.07	3.40

Table 6
Adsorption results of PB for the salt lake brine

	Li^+	Na^+	K^+	Mg^{2+}	Rb^+	Cs^+
C_0 (mol L^{-1})	2.746	1.068	0.639	0.725	8.40×10^{-3}	7.95×10^{-3}
C_e (mol L^{-1})	2.733	1.056	0.679	0.722	3.58×10^{-3}	–

"–" not detected.

hydration cation radius of the alkali ions was ranked by Cs^+ (3.25 Å) < Rb^+ (3.29 Å) < K^+ (3.31 Å) < Na^+ (3.58 Å) < Li^+ (3.82 Å) [11,15,28]. Therefore, Rb^+ was more prone to the K^+-exchange reaction, while Cs^+ was more prone to the H^+-exchange reaction due to the ion sieve effect.

3.5. Adsorption behaviors for salt lake brine

From Table 6, the concentration of metal ions except K^+ decreased after adsorption, the reduction very small for Li^+, Na^+ and Mg^{2+}, more than doubled for Rb^+. Cs^+ was not detected after adsorption equilibrium in salt lake brine. It was indicated that the adsorption ability of PB increased in the order of $Cs^+ > Rb^+ > Li^+ \sim Na^+ \sim Mg^{2+} > K^+$. PB could be used to recover Cs^+ from the salt lake brine.

4. Conclusions

The adsorption of Li^+, Na^+, K^+, Rb^+ and Cs^+ had been studied for the single-element and multi-element systems using prepared PB. The adsorption capacity followed the sequence of $Cs^+ > Rb^+ > Na^+ >> Li^+ \sim K^+$. Na^+, Rb^+ and Cs^+ in single-element and multi-element systems were in good agreement with the pseudo-second-order kinetics model, indicating that the chemisorption was the rate-limiting step. The isotherm studies indicated that Na^+ matched the Langmuir model well acting as single layer adsorption while Rb^+ and Cs^+ matched the Freundlich model by multi-layer adsorption.

The mechanism of Na^+, Rb^+ and Cs^+ adsorption onto PB was ion exchange with K^+ and H^+ existing PB crystals quantitatively demonstrated by the equation ΔC (M^+) = ΔC (K^+) + ΔC (H^+). As a result of the sieve effect in the ion exchange, Rb^+ was similar to K^+ in physicochemical properties leading to the selectivity sequence of $Rb^+ > Cs^+ > Na^+$ for ion exchange with K^+, whereas the sequence for ion exchange with H^+ was $Cs^+ > Rb^+ > Na^+$ owing to the size of hydration cation radius. The mechanism of ion pairs incorporation into PB lattice was denied on account of the unchanged concentration of Cl^- after adsorption.

Acknowledgment

We would like to thank the Natural Science Youth Foundation of Jiangsu Province (No. BK20191051), Jiangsu Province college students' innovation and entrepreneurship training program (202111049375, 202111049154) and Opening Funding of Jiangsu Provincial Engineering Laboratory for Advanced Materials of Salt Chemical Industry (No: SF201505).

References

[1] S. Yan, J. Sun, Assessing China's salt lake resources R&D based on bibliometrics analysis, Scientometrics, 105 (2015) 1141–1155.
[2] Z. Xu, M. Rong, Q. Meng, H. Yao, S. Ni, L. Wang, H. Xing, H. Qu, L. Yang, H. Liu, Fabrication of hypercrosslinked hydroxyl-rich solid phase extractants for cesium separation from the salt lake brine, Chem. Eng. J., 400 (2020) 125991, doi: 10.1016/j.cej.2020.125991.
[3] L. Gao, G. Ma, Y. Zheng, Y. Tang, G. Xie, J. Yu, B. Liu, J. Duan, Research trends on separation and extraction of rare alkali metal from salt lake brine: rubidium and cesium, Solvent Extr. Ion Exch., 38 (2020) 753–776.
[4] J. Zhang, L. Yang, T. Dong, F. Pan, H. Xing, H. Liu, Kinetics-controlled separation intensification for cesium and rubidium isolation from salt lake brine, Ind. Eng. Chem. Res., 57 (2018) 4399–4406.
[5] Y. Wu, C. Lee, H. Mimura, X. Zhang, Y. Wei, Stable solidification of silica-based ammonium molybdophosphate by allophane: application to treatment of radioactive cesium in secondary solid wastes generated from fukushima, J. Hazard. Mater., 341 (2018) 46–54.
[6] H. Lee, H. Kim, H. Jeong, M. Park, D. Chung, K. Lee, E. Lee, W. Lim, Selective removal of radioactive cesium from nuclear waste by zeolites: on the origin of cesium selectivity revealed by systematic crystallographic studies, J. Phys. Chem. C, 121 (2017) 10594–10608.
[7] M. Soliman, G. Rashad, M. Mahmoud, Fast and efficient cesium removal from simulated radioactive liquid waste by an isotope dilution-precipitate flotation process, Chem. Eng. J., 275 (2015) 342–350.
[8] T. Jellicoe, J. Richter, H. Glass, M. Tabachnyk, R. Brady, S. Dutton, A. Rao, R. Friend, D. Credgington, N. Greenham, M. Böhm, Synthesis and optical properties of lead-free cesium tin halide perovskite nanocrystals, J. Am. Chem. Soc., 138 (2016) 2941–2944.
[9] T. Sun, Z. Zheng, J. Chen, J. Wang, C. Xu, Efficient co-extraction of strontium and cesium from nitric acid medium by mixtures of di-*tert*-butylcyclohexano-18-crown-6 and 1,3-di(2-propoxy) calix[4]arene-crown-6 in *n*-octanol, Sep. Sci. Technol., 53 (2018) 503–512.
[10] S. Liu, H. Liu, Y. Huang, W. Yang, Solvent extraction of rubidium and cesium from salt lake brine with t-BAMBP-kerosene solution, Trans. Nonferrous Met. Soc. China, 25 (2015) 329–334.
[11] F. Chen, G. Jin, S. Peng, X. Liu, J. Tian, Recovery of cesium from residual salt lake brine in Qarham playa of Qaidam Basin with prussian blue functionalized graphene/carbon fibers composite, Colloids Surf., A, 509 (2016) 359–366.
[12] J. Su, G. Jin, T. Chen, X. Liu, C. Chen, J. Tian, The characterization and application of prussian blue at graphene coated carbon fibers in a separated adsorption and electrically switched ion exchange desorption processes of cesium, Electrochim. Acta, 230 (2017) 399–406.
[13] S. Manabe, V. Kiliyankil, T. Kumashiro, S. Takiguchi, B. Fugetsu, I. Sakata, Stabilization of Prussian blue using copper sulfate for eliminating radioactive cesium from a high pH solution and seawater, J. Hazard. Mater., 386 (2020) 121979.
[14] H. Wi, H. Kim, D. Oh, S. Bae, Y. Hwang, Surface modification of poly(vinyl alcohol) sponge by acrylic acid to immobilize Prussian blue for selective adsorption of aqueous cesium, Chemosphere, 226 (2019) 173–182.
[15] C. Thammawong, P. Opaprakasit, P. Tangboriboonrat, P. Sreearunothai, Prussian blue-coated magnetic nanoparticles for removal of cesium from contaminated environment, J. Nanopart. Res., 15 (2013) 1689.
[16] B. Hu, B. Fugetsu, H. Yu, Y. Abe, Prussian blue caged in spongiform adsorbents using diatomite and carbon nanotubes for elimination of cesium, J. Hazard. Mater., 217–218 (2012) 85–91.
[17] M. Ishizaki, S. Akiba, A. Ohtani, Y. Hoshi, K. Ono, M. Matsuba, T. Togashi, K. Kananizuka, M. Sakamoto, A. Takahashi,

T. Kawamoto, H. Tanaka, M. Watanabe, M. Arisaka, T. Nankawa, M. Kurihara, Proton-exchange mechanism of specific Cs^+ adsorption via lattice defect sites of Prussian blue filled with coordination and crystallization water molecules, Dalton Trans., 42 (2013) 16049–16055.
[18] H. Yang, L. Sun, J. Zhai, H. Li, Y. Zhao, H. Yu, In situ controllable synthesis of magnetic Prussian blue/graphene oxide nanocomposites for removal of radioactive cesium in water, J. Mater. Chem. A, 2 (2014) 326–332.
[19] D. Vu Ca, J.A. Cox, Solid phase extraction of cesium from aqueous solution using sol-gel encapsulated cobalt hexacyanoferrate, Microchim. Acta, 147 (2004) 31–37.
[20] L. Lin, X. Huang, L. Wang, A. Tang, Synthesis, characterization and the electrocatalytic application of prussian blue/titanate nanotubes nanocomposite, Solid State Sci., 12 (2010) 1764–1769.
[21] H. Buser, D. Schwarzenbach, W. Petter, A. Ludi, The crystal structure of Prussian blue: $Fe_4[Fe(CN)_6]_3 \cdot xH_2O$, Inorg. Chem., 16 (1977) 2704–2710.
[22] Q. Song, Y. Fang, Z. Liu, L. Li, Y. Wang, J. Liang, Y. Huang, J. Lin, L. Hu, J. Zhang, C. Tang, The performance of porous hexagonal BN in high adsorption capacity towards antibiotics pollutants from aqueous solution, Chem. Eng. J., 325 (2017) 71–79.
[23] C. Futalan, C. Kan, M. Dalida, K. Hsien, C. Pascua, M. Wan, Comparative and competitive adsorption of copper, lead, and nickel using chitosan immobilized on bentonite, Carbohydr. Polym., 83 (2011) 528–536.
[24] G. Li, Y. Huang, J. Lin, C. Yu, Z. Liu, Y. Fang, Y. Xue, C. Tang, Effective capture and reversible storage of iodine using foam-like adsorbents consisting of porous boron nitride microfibers, Chem. Eng. J., 382 (2020) 122833.
[25] R. Wilde, S. Ghosh, B. Marshall, The Prussian blues, Inorg. Chem., 9 (1970) 2512–2516.
[26] A. Vipin, B. Hu, B. Fugetsu, Prussian blue caged in alginate/calcium beads as adsorbents for removal of cesium ions from contaminated water, J. Hazard. Mater., 258–259 (2013) 93–101.
[27] T. Simonsson, R. Sjoback, DNA tetraplex formation studied with fluorescence resonance energy transfer, J. Biol. Chem., 274 (1999) 17379.
[28] E. Nightingale Jr., Phenomenological theory of ion solvation. Effective radii of hydrated ions, J. Phys. Chem., 63 (1959) 1381–1387.